

Long photometric cycle and disk evolution in the β Lyrae type binary OGLE-BLG-ECL-157529

R.E. Mennickent¹, J. Garcés¹, G. Djurašević^{2,3}, P. Iwanek⁴, D. Schleicher¹, R. Poleski⁴, and I. Soszyński⁴

¹ Universidad de Concepción, Departamento de Astronomía, Casilla 160-C, Concepción, Chile
e-mail: rmennick@udec.cl

² Astronomical Observatory, Volgina 7, 11060 Belgrade 38, Serbia

³ Issac Newton institute of Chile, Yugoslavia Branch, 11060, Belgrade, Serbia

⁴ Astronomical Observatory, University of Warsaw, Al. Ujazdowskie 4, PL-00-478 Warszawa, Poland

Received XX XX, 2020; accepted XX XX, 2020

ABSTRACT

Context. The subtype of hot algol semidetached binaries dubbed Double Periodic Variables (DPVs) are characterized by a photometric cycle longer than the orbital one, whose nature has been related to a magnetic dynamo in the donor component controlling the mass transfer rate.

Aims. We aim to understand the morphologic changes observed in the light curve of OGLE-BLG-ECL-157529 that are linked to the long cycle. In particular, we want to explain the changes in relative depth of primary and secondary eclipses.

Methods. We analyze *I* and *V*-band OGLE photometric times series spanning 18.5 years and model the orbital light curve.

Results. We find that OGLE-BLG-ECL-157529 is a new eclipsing Galactic DPV of orbital period 24^d.8, and that its long cycle length decreases in amplitude and length during the time baseline. We show that the changes of the orbital light curve can be reproduced considering an accretion disk of variable thickness and radius, surrounding the hottest stellar component. Our models indicate changes in the temperatures of hot spot and bright spot during the long cycle, and also in the position of the bright spot. This, along with the changes in disk radius might indicate a variable mass transfer in this system.

Key words. stars: binaries (including multiple), close, eclipsing - stars: variables: general - accretion: accretion disks

1. Introduction

Double Periodic Variables (DPVs) are a subset of Algol-type binary systems. They consist of a red giant that has filled its Roche lobe and transfers material through an optically thick accretion disk onto a B-type dwarf. Its main characteristic is that they have two photometric cycles: a short period P_o , whose light curve shape is typical of the orbital modulation in eclipsing or ellipsoidal binaries and a long cycle period P_l , whose origin is still unknown. Both periodicities are related through the relationship $P_l = 33 \times P_o$, but the period ratio for a particular case can differ considerably from the average (Mennickent et al. 2003; Poleski et al. 2010; Pawlak et al. 2013; Mennickent, Otero & Kołaczowski 2016; Mennickent 2017). In some systems, a decrease in the long period has been reported, as in the case of OGLE-LMC-DPV-065 (Poleski et al. 2010; Mennickent et al. 2019) and OGLE-LMC-DPV-056 (Mennickent et al. 2008).

A magnetic origin has been proposed as the cause of the long cycle (Schleicher & Mennickent 2017). The rapid rotation of an orbitally synchronized donor star, added to the convective motions would cause it to have a magnetic dynamo, which would change the equatorial stellar radius as indicated by the Applegate's mechanism (Applegate & Patterson 1987; Applegate 1992) which should modulate the mass transfer through the inner Lagrangian point. These changes could be observed as cyclic luminosity variations evidenced in the long cycle. This model, proposed by Schleicher & Mennickent (2017), predicts the correlation between the orbital and long periods and also the value of the long cycle length for particular systems with rela-

tively good accuracy; for the seven studied binaries with orbital periods between 5 and 13 days, the maximum deviation between predicted and observed ratio is 30%, with the average deviation of the order of 12%. Actually, it has been shown that rapid rotation favors the operation of the Applegate's mechanism (Navarete et al. 2018).

Other mechanisms have been identified as drivers for mass transfer changes in close binaries. These include direct modulation of mass transfer through the magnetic field of the donor star (Bolton 1989; Meintjes 2004) and the effect of star spots or prominences (Livio & Pringle 1994; Steeghs, et al. 1996; Meintjes 2004).

Recently, Mg II, Fe I, Fe II, C I and Ti II emission lines that are signatures of chromospherically active stars were detected in V 393 Scorpii, supporting the existence of magnetically active donors in DPVs (Mennickent, Schleicher & San Martín-Pérez 2018). In addition, magnetic fields have been inferred in β Lyrae from the analysis of polarized light that could produce magnetically driven streams onto the accretion disk (Skulskij 1982, 2018).

Significant changes have been detected in the morphology of the light curve of OGLE-LMC-DPV-097 that are directly related to the long cycle (Garcés et al. 2018). These authors show that this kind of variability could be due to physical changes of the accretion disk, which would change its diameter and thickness cyclically according to the phase of the long cycle. If the long cycle reflects changes in the mass transfer rate, we might expect changes in disk properties too, since the disk interacts with the gas stream.

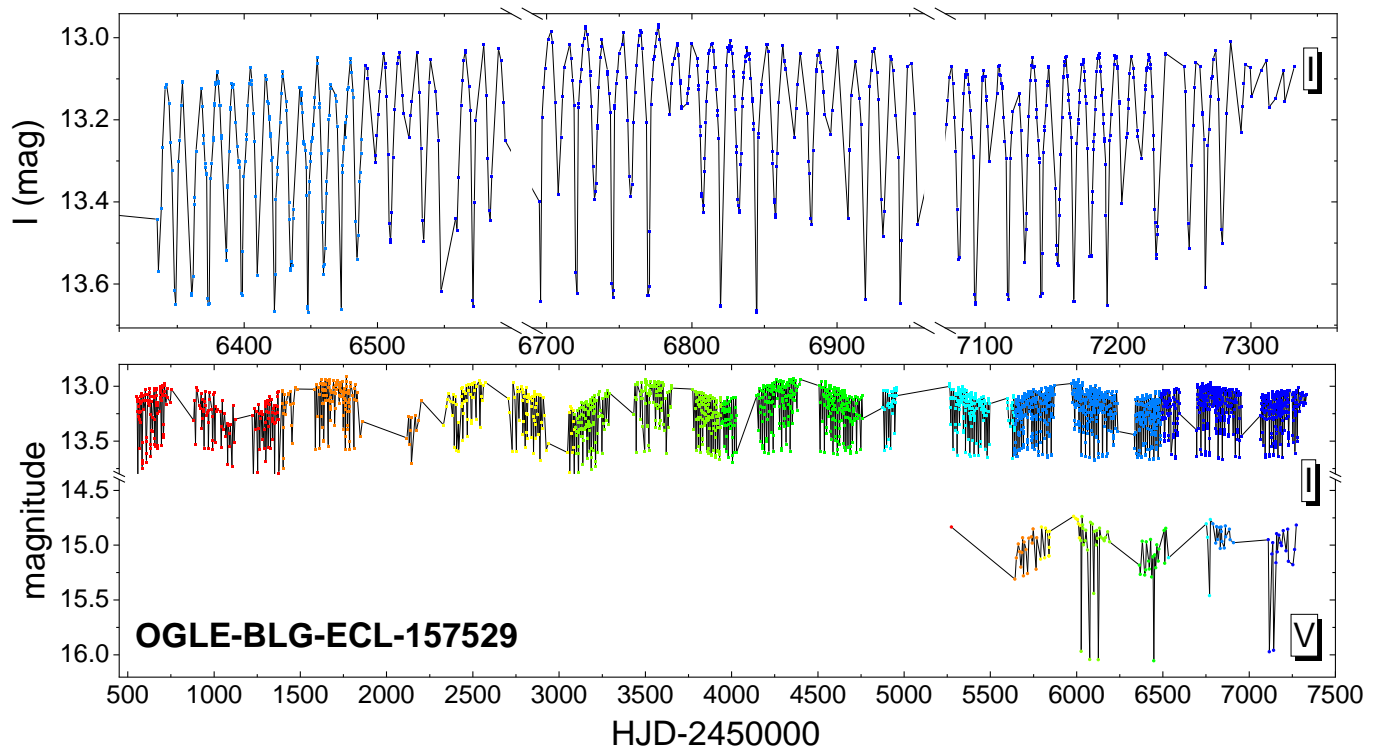


Fig. 1. The OGLE *I* and *V*-band light curves of OGLE-BLG-ECL-157529. Colors indicate different data ranges.

In this study we show the photometric analysis of a Galactic DPV binary system that presents a variable long cycle, viz. OGLE-BLG-ECL-157529 ($\alpha_{2000}=17:53:08.33$, $\delta_{2000}=-32:46:27.0$, $I=13.035$ mag, $V=14.829$ mag, Soszyński et al. (2016)). It is the first DPV reported in the direction of the Galactic bulge. The Gaia DR2 identification is 4043437999622564608 and its parallax is 0.331 ± 0.044 mas, implying a distance of 3024 ± 406 pc (Gaia Collaboration et al. 2016, 2018). This distance fits well to that provided by Bailer-Jones et al. (2018), viz. 2815 pc with lower limit at 2487 pc and upper limit at 3240 pc. The above indicates that the system is not a member of the Galactic bulge, but a foreground star.

We used good time coverage in OGLE data to study changes in the morphology of the light curve. It occurred that they are, similarly to OGLE-LMC-DPV-097, related to the long cycle. Our motivation is to investigate the physical phenomena that give rise to the peculiar changes observed in its orbital light curve, in order to understand the cause of these changes. This object, together with other DPVs that show linked orbital and long cycle variability, could be fundamental in a study aimed to understand the DPV phenomenon and test the hypothesis of the magnetic dynamo. A preliminary report of this investigation was presented by Garcés et al. (2019).

2. Photometric Data

This object is included in the catalogue of eclipsing binaries in the Galactic bulge presented by Soszyński et al. (2016). The photometric time series analyzed in this study consists of 2606 *I*-band data points taken from the following data bases (Fig. 1): OGLE-II (Szymański 2005)¹ and OGLE-III/IV². The OGLE-IV project is described by Udalski, Szymański, & Szymański

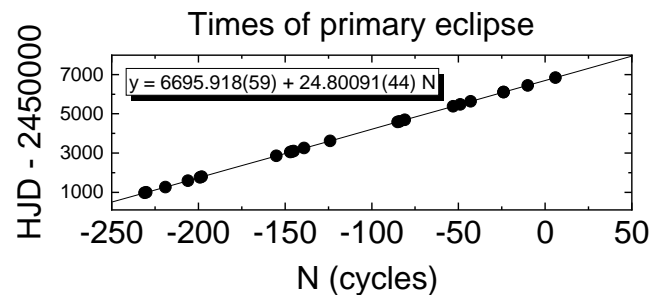


Fig. 2. Times of primary eclipse provide an improved value for the orbital period $24^{\text{d}}80091 \pm 0^{\text{d}}00044$.

Table 1. Summary of photometric observations. The number of measurements, starting and ending times, and average magnitude are given. $HJD' = HJD - 2450000$. The uncertainty of a single measurement varies between 4 and 6 mmag.

band/Data-Base	N	HJD'_{start}	HJD'_{end}	Mag
I / OGLE-II	346	551.77073	1858.52147	13.213
I / OGLE-III	795	2117.76494	4955.73490	13.221
I / OGLE-IV	1465	5261.84891	7332.50545	13.213
V / OGLE-IV	118	5274.88451	7273.60682	15.038

(2015). In addition, the OGLE-IV data base provides 118 additional *V*-band measurements. The whole dataset, summarized in Table 1, spans a time interval of 6781 d, i.e. 18.5 yr.

3. Light curve analysis

The light curve shows alternate and periodic minima that are typical of an eclipsing binary system, but also a long cycle in time scale of several hundreds of days (Fig. 1). The system is fainter

¹ <http://ogledb.astrouw.edu.pl/~ogle/photdb/>

² OGLE-III/IV data kindly provided by the OGLE team.

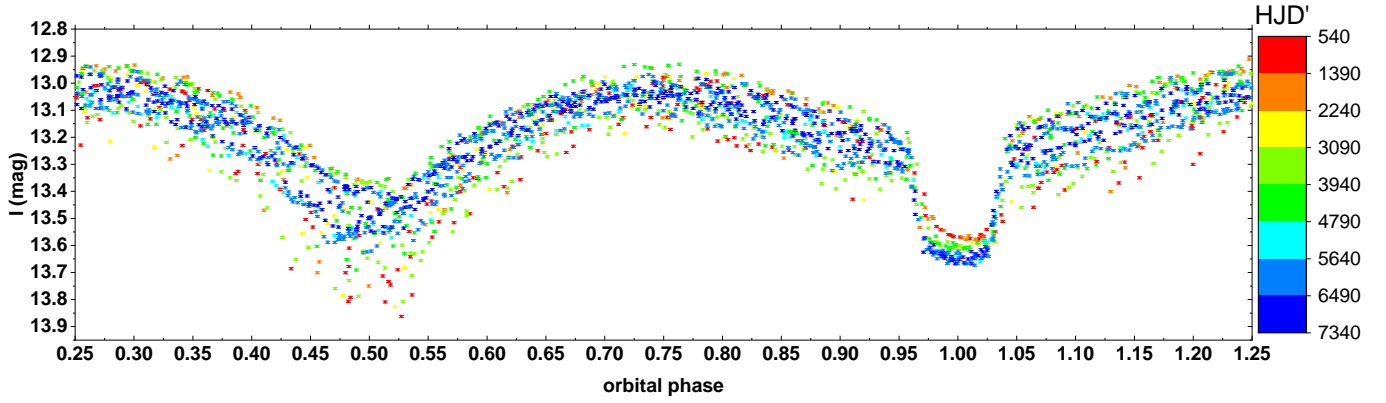


Fig. 3. The OGLE *I*-band light curve of OGLE-BLG-ECL-157529 phased with the ephemeris given by Eq. 1. Colors label data shown in Fig. 1.

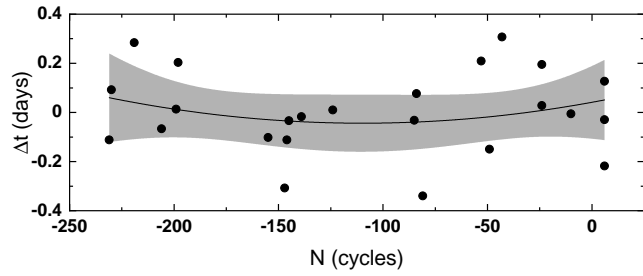


Fig. 4. Observed minus calculated times for primary eclipses using the orbital period given by the ephemeris of Eq. (1) and the best fit. Dashed area shows the 95% confidence band.

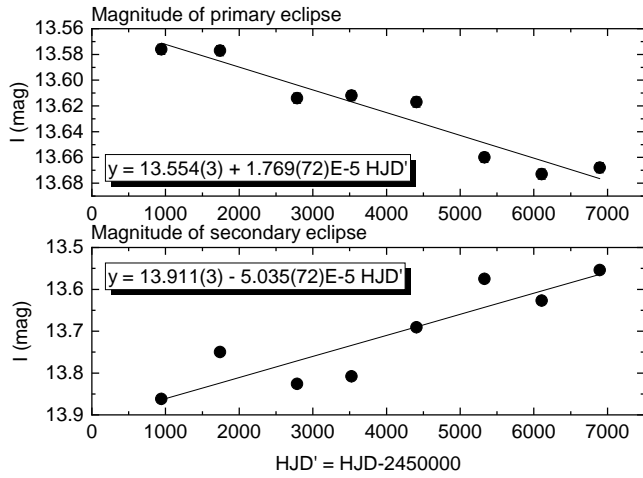


Fig. 5. Eclipse magnitudes as a function of time. The lowest point of every colored data segment in the eclipses of Fig. 2 is plotted.

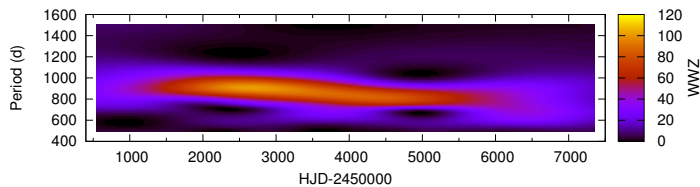


Fig. 6. The WWZ 2D power spectrum as a function of period and time.

in the *V*-band than in the *I*-band and the eclipses are deeper in *V*.

We used the generalized Lomb-Scargle (GLS) periodogram to obtain the orbital frequency in our data. This algorithm was

introduced by Zechmeister & Kürster (2009) and uses the principle of the Lomb (1976) & Scargle (1982) periodograms with some modifications, such as the addition of a displacement in the adjustment of the fit function and the consideration of measurement errors. Compared with the classical periodogram, it gives us more accurate frequencies and a better determination of the amplitudes. We obtained $P_0 = 24^d7992 \pm 0^d0024$.

With the above period we phased the *I*-band light curve. This allowed us to select the deeper data points in the primary eclipse, corresponding in this system to the usually more deeper eclipse, for every data segment that is colored in Fig. 1. These data points were analyzed with the cycle-number technique for linear-ephemerides (Sterken 2005) and the following improved ephemeris for the primary eclipse was derived (Fig. 2):

$$\text{HJD} = (245\,6695^d918 \pm 0^d059) + (24^d80091 \pm 0^d00044) E \quad (1)$$

where N is the cycle number. This period was used to phase the light curve shown in Fig. 3. From this figure we infer the following: (1) at some epochs the secondary eclipse becomes deeper than the primary eclipse, (2) the secondary eclipse has larger variability (scatter) than the primary eclipse, (3) the regularity of time strings reflected in colored data suggests that the non-orbital variability occurs mostly in time scales of hundred of days, (4) while the secondary eclipse changes its depth as well as its width, the primary one make it primarily in depth, and with less amplitude than the secondary eclipse, (5) the long cycle, revealed by the scattered data, becomes more evident outside the primary eclipse, suggesting that the light source becomes at least partially eclipsed during primary eclipse, (6) there is a tendency for the primary eclipse in being deeper with time, and (7) the orbital period seems to be very stable during the observing period.

We tested the last statement making an analysis of the times of primary eclipse with the "period-change equation" (Percy et al. 1980). This method assumes a constant rate of change of the period and compares predicted times with observed times in a similar way that the O-C diagram described by Sterken (2005) does it. As eclipse timings we choose the fainter points in the colored data strings shown in Fig. 3. We find a period rate of change of $dP_0/dt = (1.41 \pm 1.38) \times 10^{-5} \text{ d d}^{-1}$, i.e. the period is constant for all practical purposes (Fig. 4).

We find that the eclipses depth changes linearly with time and in opposite way on the 18.5-year interval; the total change of the secondary eclipse depth, viz. about 0.35 mag, is larger than the total change of the primary eclipse depth, viz. about 0.10 mag (Fig. 5).

The long cycle is revealed in the Weighted Wavelet Z transform (WWZ) as defined by Foster (1996). The WWZ works

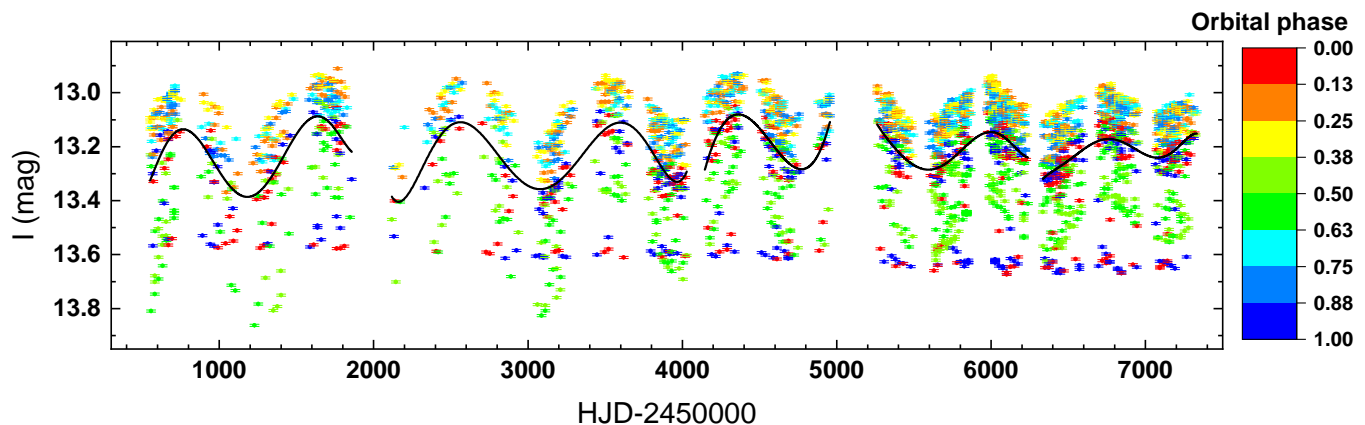


Fig. 7. The I -band light curve showing the polynomial fits to the long cycle. Colors represent the orbital phases according to the ephemeris given by Eq. 1. Note the evolution of the secondary eclipse (green) and the primary eclipse (red and blue).

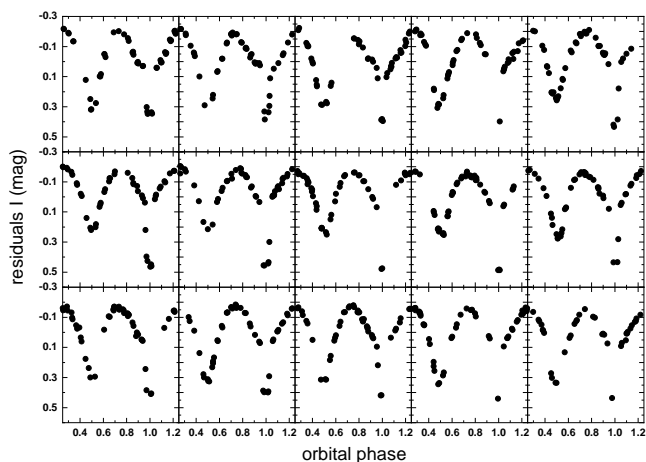


Fig. 8. Orbital light curves constructed with residuals of the fits shown in Fig. 7 for data spanning the time interval (HJD-245000) between 6334.9 and 7332.5. Every panel shows 50 consecutive data points. Time goes from left to right from upper left to lower right panel.

similarly as the Lomb-Scargle periodogram providing information about the periods of the signal and the time associated to those periods. It is very suitable for the analysis of non-stationary signals and has advantages in the analysis of time-frequency local characteristics. The WWZ shows the long period decreasing from around 900 days to around 800 days through the time baseline (Fig. 6).

We fit data segments with order-6 polynomials in order to represent the long cycle. These fits show that the long cycle decreases its period and amplitude during the time baseline (Fig. 7). It is clear from this figure the continuous smooth decrease of the brightness of the primary eclipse (lower red and blue points, orbital phases around 0 or 1) along with the much fainter secondary eclipses occurring at some epochs (green very low points, orbital phases around 0.5). It is also clear how the secondary eclipse becomes brighter as time goes by.

We analyzed the orbital light curves after removing the long cycle. This was done using the residuals of the fits shown in Fig. 7. Examples of "cleaned" orbital light curves are shown in Fig. 8. These show changes in the shape of the orbital light curve which are more evident during the first observing epochs (Fig. 9). In particular, we notice the changes in the shape of the eclipses and the ingress and egress light curve branches. The pri-

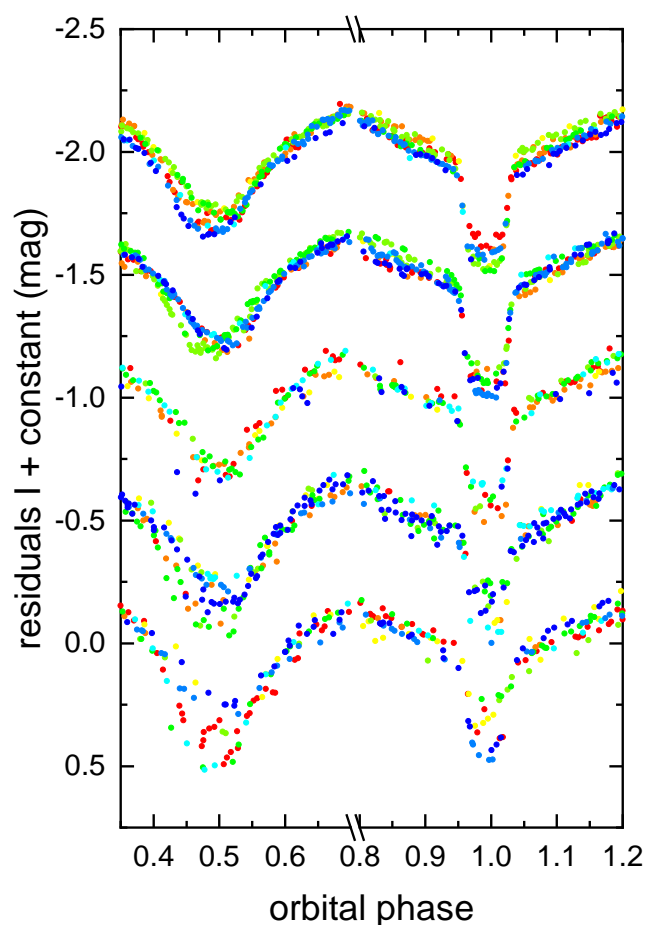


Fig. 9. Orbital light curves constructed with the residuals of the fits shown in Fig. 7. Data are grouped for the first fit (lower) until the fifth fit residuals (upper). To illustrate changes in the shape of the light curves, data are marked with a color map following the HJD; red for the first observations and blue for the last observations of every segment.

mary eclipse is not always deeper than the secondary one, this is specially evident in the first observing epochs. We also notice changes in the shape of the light curve during epochs of long cycle maximum and minimum (Fig. 10); during the minima of the long cycle occurs the reversals of the eclipse depths, something already visible in Fig. 7 at the lower parts of the fits.

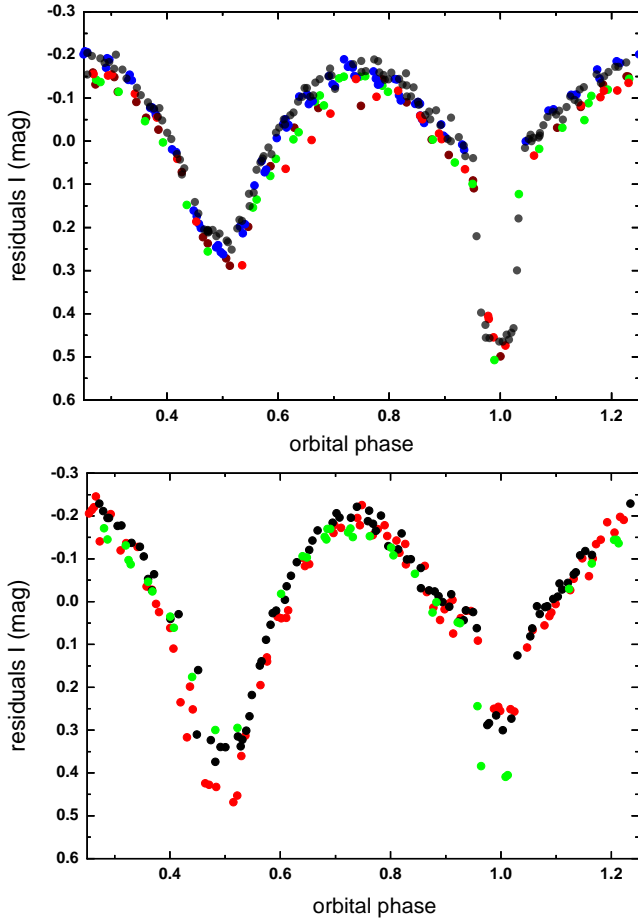


Fig. 10. Orbital light curves constructed with the residuals of the fits shown in fig. 5. Data are grouped for times of maxima (upper) and minima (lower) of the long cycle. The ranges of HJD - 2450000 are: (Upper) brown; 3569.8-3629.6, green; 4329.6-4393.5, blue; 5866.5-6023.8, red; 1608.8-1667.8 and black; 6572.6-6816.8, (Lower) red; 3049.9-3205.6, black; 3881.7-4028.5 and green; 7064.9-7110.9.

In order to understand these changes we investigate in the next section the nature of the star facing the observer during the primary eclipse. This is usually named donor star in a β -Lyr type binary, because it transfer mass onto the "gainer" star through a gas stream flowing from its inner Lagrangian point.

3.1. On the system reddening, distance and donor star

Since we do not have spectroscopic data for our object, we must rest in the photometry to further understand the system. Using the OGLE-IV photometry and the disentangled orbital light curve, we obtain a $V - I = 2.42$ mag at the primary eclipse. The location of this DPV in the direction of the Galactic bulge causes that the light from this object is strongly reddened by unevenly distributed interstellar matter.

This object is located in the OGLE field BLG535, which is distant from the Galactic plane by slightly over 3 degrees. In this direction dust is distributed highly non-uniformly and reddening changes on a small angular scale. Nataf et al. (2013) have estimated reddening using red clump stars located in the Galactic bulge, so reddening measurements from Nataf's map are the upper limits toward analyzed directions, and they should not be used straightforward for the objects located definitely closer than the Bulge. In Fig. 11 we show a color-magnitude diagram

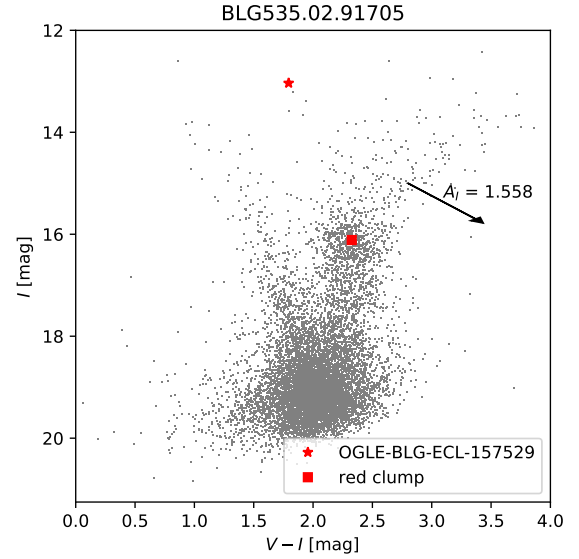


Fig. 11. color-magnitude diagram for stars surrounding OGLE-BLG-ECL-157529. The reddening vector, extinction value and magnitudes of the red clump are from Nataf et al. (2013). More details can be found in Section 3.1.

(CMD) towards the direction of the OGLE-BLG-ECL-157529. We use stars located in the radius of about 2.5 arcmin around the position of the analyzed object. In the CMD we mark our target, the red clump (which has mean position: $((V - I), I) = (2.33$ mag, 16.11 mag) and the reddening vector. We use the OGLE Extinction Calculator³ that uses the Nataf's extinction maps, and obtain limit for the color excess $E(V - I) = 1.266$ mag using the nearest method and $E(V - I) = 1.248$ mag using the natural neighbor method.

As previously mentioned, the Gaia parallax of 0.33065 ± 0.04436 mas implies a distance of $d = 3024 \pm 406$ pc. This means that the object is in the Galactic disk and not in the Bulge. Using the Recio-Blanco model for the Galactic disk (Recio-Blanco et al. 2014) along with the Gaia distance we obtain $E(V - I) = 0.945$ mag implying a dereddened color index of $(V - I)_0 = 1.475$ mag at the primary eclipse. In the previous step we used as input the uncorrected color excess obtained with the natural neighbor method. To complement our research on reddening, we used also the Python package named "mwdust"⁴ that uses several existing extinction maps in the Milky Way (Bovy et al. 2016). Using this package, we obtain extinction at a given direction and distance. For the distance 3.02 kpc we have obtained extinction in V - and I -band $A_V = 2.288$ mag and $A_I = 1.256$ mag, what gives $E(V - I) = 1.033$ mag roughly confirming the earlier calculation.

The corrected color in primary eclipse obtained with the Recio-Blanco model (Recio-Blanco et al. 2014), viz. $(V - I)_0 = 1.47$ mag, corresponds to a K2-type star with $T_c = 4400$ K (Drilling & Landolt 2000) (Fig. 12). In the following we will assume that this is the effective temperature of the donor star. The relative stability of the primary eclipse might support this conjecture.

³ <http://ogle.astrouw.edu.pl/cgi-ogle/gettext.py>

⁴ <https://github.com/jobovy/mwdust>

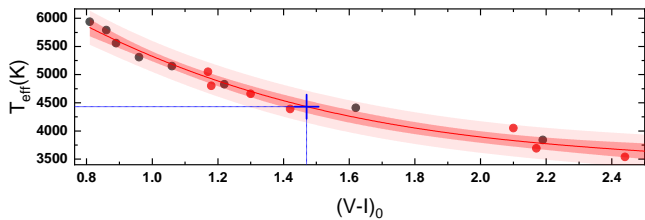


Fig. 12. Temperature versus color for dwarfs (black dots) and giants (red dots) from Drilling & Landolt (2000) and the best 3th order polynomial fit. 95% confidence and prediction bands are shown by dashed and dashed-light areas, respectively. The position of OGLE-BLG-ECL-157529 during primary eclipse is also shown.

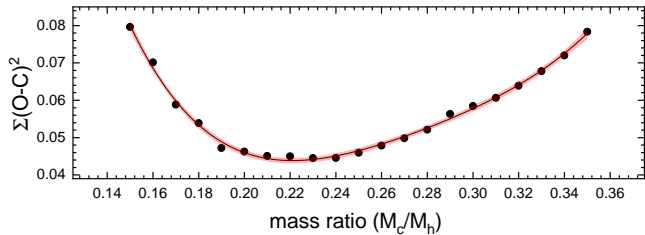


Fig. 13. The parameter $\Sigma (O-C)^2$ for the fits done to the light curve with data obtained at the maximum of the long cycle, as a function of mass ratio. The best 4th order polynomial fit is shown along with the 95% confidence band.

4. Discussion

4.1. Overall qualitative interpretation

The overall behavior of the light curve, especially the behavior of the secondary eclipse, can be interpreted in the terms of circumstellar material in the system. The changing shape of the secondary eclipse cannot be due to occultation by a star, but by a variable structure such as an accretion disk, surrounding the more massive star and formed by mass transfer from the Roche lobe overflow of the less massive star. This configuration is typical of semidetached Algols of the β Lyrae type. What is not typical and it is unique for this system is the presence of a large amplitude long photometric cycle and the remarkable changes observed in the relative depths of the primary and secondary eclipses.

From the analysis shown in the previous section we might infer the existence of a large disk during the first observing epochs, but that decreases its size when time goes by. This should explain why the secondary eclipse is deeper on the beginning. This long-term behavior of the disk is reflected in the secondary eclipse magnitude (Fig. 5). When the disk is vertically larger (regarding the orbital plane), it occults a larger fraction of the donor and gainer and the eclipse becomes deeper. However, the deeper secondary eclipses occurs only during long-cycle minima, and this should indicate that the disk size is also modulated by the long cycle, but in a shorter time scale compared with the aforementioned decade-length secular tendency.

We also notice that the disk attains maximum size when the long cycle has larger amplitude and its cycle length is longer, i.e. at the beginning of the time series. We suggest that changes in mass transfer controls the disk size and eventually the brightness of the extra source responsible of the long cycle. This extra source might be a hot spot wind as suggested for the DPV system V 393 Scorpii (Mennickent et al. 2012) and also for β Lyrae (Harmanec, et al. 1996). Since we don't detect changes in the

orbital period, the mass transfer in this system should be rather small.

4.2. Light curve model

In this subsection we model the light curve in order to test the picture of the variable disk given above. For that we use a theoretical code that solves the inverse problem and that considers a system consistent of a donor star and a gainer star surrounded by an accretion disk, that is both optically and geometrically thick (Djurašević 1992a,b, 1996). The disk temperature is the same that the gainer in its inner edge and decreases with a radial profile described by an exponent a_T . The model includes a hot spot and a bright spot in the disk, following evidence found in previous observations of algols (Richards 2004). These active regions influence the shape of the light curve during the ingress and egress of the eclipses. The model has been described in detail in several papers, so we remit the interested reader to Mennickent & Djurašević (2013); Mennickent et al. (2015, 2019). We assume a donor temperature $T_c = 4400$ K, as derived in the previous section. We also assume synchronous rotation for the donor, as expected for a close binary that rapidly synchronize stellar spins with the orbit due to tidal forces. On the other hand, the gainer might have been spun-up to a high rotation due to nearly tangentially infalling material (Packet 1981), hence we have assumed critical rotation for this star. We find that our model is practically the same for synchronous and critical gainer.

We use the q-search method, usually applied to over-contact or semi-detached binaries when no spectroscopic data are available (Terrell & Wilson 2005). We find convergent solutions for a range of mass ratios $q = M_c/M_h$, where the subindexes "c" and "h" refer to the cool and hot stars. A fit with a fourth order polynomial to the corresponding $\Sigma (O - C)^2$ values, yields an optimal mass ratio $q = 0.22$ (Fig. 13). Previous studies show $\bar{q} = 0.23 \pm 0.05$ (standard deviation) for the few studied DPVs (Mennickent, Otero & Kołaczowski 2016). For the q-search we used data obtained at maximum (Fig. 10 upper), when the disk influence should be lower, as discussed in the previous section.

Next we model the light curve at data ranges representative of the maximum and minimum of the long cycle. We choose those data ranges that best represent the observed differences between maximum and minimum, where the inversion of the eclipses is more evident. The parameters of the fits are shown in Table 2 and a comparison of our theoretical models and observations is given in Fig. 14. While the models reproduce relatively well the general appearance of the light curves, the fit at minimum has more scatter than at maximum. It is possible that at minimum the emissivity sources are more complex and our simple model of disk plus spots cannot reproduce so well the overall system emissivity.

4.3. Discussion of the light curve models

Our model indicates a system seen at angle 85° and a stellar separation of $65 R_\odot$. The stellar temperatures are 4400 K and $14,000$ K. The stellar masses are 4.83 and $1.06 M_\odot$ and surface gravities $\log g = 3.86$ and 2.02 . The stellar radii are 4.5 and $16.6 R_\odot$. The gainer has a surface temperature indicating a spectral type B 6 (Harmanec 1988), consistent with the B-type spectral types found in DPV gainers. Although we have justified the use of the fixed parameters T_c and q , the stellar parameters might be refined when spectroscopic data come to be available.

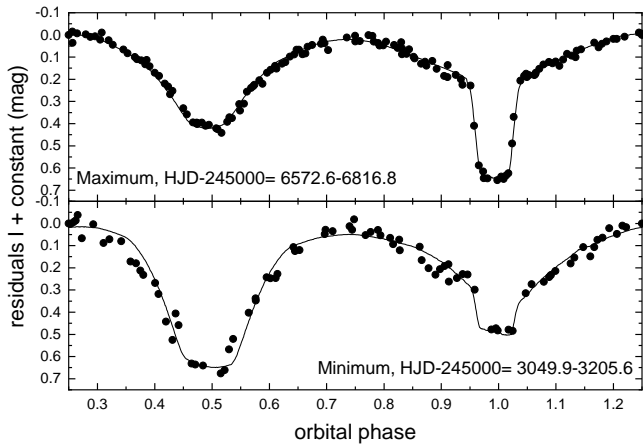


Fig. 14. Orbital light curves at long cycle maximum and minimum along with the fits provided by the models described in Table 2.

Significant differences are observed in disk properties when passing from maximum to minimum of the long cycle: the radius increases from 27 to 33 R_{\odot} , while the temperature at the outer edge remains around 3000-3500 K. The vertical thickness at the outer edges increases from 3 to 11 R_{\odot} , which explains the inversion of the eclipse depths. The average disk radius of 30 R_{\odot} means $R_d/a \approx 0.47$, i.e. the disk outer border is just below the tidal radius for the given mass ratio (Paczynski 1977; Warner 1995a). This opens the possibility that at minimum the outer disk, especially optically thin regions that are not tested with our light curve model, becomes influenced by tidal forces. The light contribution of the larger disk explains the shallower primary eclipse observed at the first epochs (red points in Fig. 3).

The bright spot is located roughly at the expected region where the stream impacts the disk, 47° apart from the lines joining the stellar centers in the direction of the orbital motion. This position does not change between maximum and minimum. On the contrary, the position of the bright spot changes from 66° to 125° from maximum to minimum, as measured in the opposite direction of the orbital motion. At maximum the hot spot temperature is 48% higher than the surrounding disk, at minimum is only 13% higher, in principle consistent with much kinetic energy released in the stream-disk impact region in a smaller disk. At maximum the bright spot temperature is 37% higher than the surrounding disk and 8% at minimum.

We notice that changes in disk parameters, especially disk radius and temperatures of the active regions, might indicate variable mass transfer in the system, as required in the dynamo model proposed by Schleicher & Mennickent (2017).

5. Conclusion

- We find that the eclipsing binary OGLE-BLG-ECL-157529 is a Double Periodic Variable characterized by an orbital period of $24^d 80091 \pm 0^d 00044$ and a long cycle length decreasing in length and amplitude during 18.5 years of observations.
- The overall light curves can be understood in terms of a variable accretion disk. The disk is larger and thicker at long cycle minimum and this effect is more pronounced when the long cycle has larger amplitude and longer cycle length.
- Our models indicate changes in the temperatures of hot spot and bright spot during the long cycle, and also in the position

of the bright spot. This, along with the changes in disk radius might indicate variable mass transfer in this system.

Acknowledgements. We thanks the anonymous referee who contributed to improve the first version of this manuscript. REM and JG acknowledge support by VRID-Enlace 216.016.002-1.0, BASAL Centro de Astrofísica y Tecnologías Afines (CATA) PFB-06/2007 and FONDECYT 1190621. DS and REM thank FONDECYT 1201280 and DS thanks FONDECYT 1161247. JG acknowledges ANID project 21202285 and members of stellar variability group (S.V.G. UdeC) for useful discussions about this work. GD acknowledges the financial support of the Ministry of Education, Science and Technological Development of the Republic of Serbia through the contract No 451-03-68/2020/14/20002. The OGLE project has received funding from the Polish National Science Centre grant MAESTRO no. 2014/14/A/ST9/00121. This work has made use of data from the European Space Agency (ESA) mission *Gaia* (<https://www.cosmos.esa.int/gaia>), processed by the *Gaia* Data Processing and Analysis Consortium (DPAC, <https://www.cosmos.esa.int/web/gaia/dpac/consortium>). Funding for the DPAC has been provided by national institutions, in particular the institutions participating in the *Gaia* Multilateral Agreement.

References

- Applegate J. H., 1992, *ApJ*, 385, 621
- Applegate J. H., Patterson J., 1987, *ApJL*, 322, L99
- Bailer-Jones C. A. L., Rybizki J., Fouesneau M., Mantelet G., Andrae R., 2018, *AJ*, 156, 58
- Bolton C. T., 1989, *SSRv*, 50, 311
- Bovy J., Rix H.-W., Green G. M., Schlafly E. F., Finkbeiner D. P., 2016, *ApJ*, 818, 130
- Djurašević G., 1992a, *Ap&SS*, 196, 267
- Djurašević G., 1992b, *Ap&SS*, 197, 17
- Djurašević G., 1996, *Ap&SS*, 240, 317
- Drilling, J. S., & Landolt, A. U. 2000, in *Allen's Astrophysical Quantities*, ed. A. N. Cox (4th ed.; New York: Springer), 381
- Foster G., 1996, *AJ*, 112, 1709
- Gaia Collaboration, et al., 2016, *A&A*, 595, A1
- Gaia Collaboration, et al., 2018, *A&A*, 616, A1
- Garcés L. J., Mennickent, R. E., Djurašević, G., Poleski, R., Soszyński, I. 2018, *MNRAS*, 477, 11
- Garcés J., Mennickent R. E., Djurašević G., Poleski R., 2019, *CoSka*, 49, 355
- Harmanec P., 1988, *BAICz*, 39, 329
- Harmanec P., et al., 1996, *A&A*, 312, 879
- Livio M., Pringle J. E., 1994, *ApJ*, 427, 956
- Lomb N. R., 1976, *Ap&SS*, 39, 447 L..47M
- Meintjes P. J., 2004, *MNRAS*, 352, 416
- Mennickent, R. E., 2017, *Serb. Astron. J.*, 194, 1
- Mennickent, R. E., Pietrzyński, G., Diaz, M., Gieren, W., 2003, *A&A*, 399, 47
- Mennickent, R. E., Kołaczowski, Z., Michalska, G., Pietrzyński, G., Gallardo, R., Cidale, L., Granada, A., Gieren, W., 2003, *MNRAS*, 389, 1605
- Mennickent R. E., et al., 2012b, *MNRAS*, 427, 607
- Mennickent R. E., Djurašević G., 2013, *MNRAS*, 432, 799
- Mennickent, R. E., Djurašević, G., Cabezas, M., Cséki, A., Rosales, J. G., Niemczura, E., Araya, I., Curé, M. 2015, *MNRAS*, 448, 1137
- Mennickent, R. E., Otero, S., Kołaczowski, Z. 2016, *MNRAS*, 455, 1728

Table 2. Results of the analysis of the light curves shown in Fig. 14. The parameters are obtained by solving the inverse problem for the Roche model with an accretion disk around the more massive (hotter) gainer in critical non-synchronous rotation regime (Djurašević 1992a,b, 1996).

Quantity	OGLE – max	Quantity	OGLE – max	Quantity	OGLE – min	Quantity	OGLE – min
n	142	$\mathcal{M}_h [M_\odot]$	4.83 ± 0.3	n	85	$\mathcal{M}_h [M_\odot]$	4.83 ± 0.3
$\Sigma(O - C)^2$	0.0386	$\mathcal{M}_c [M_\odot]$	1.06 ± 0.2	$\Sigma(O - C)^2$	0.1404	$\mathcal{M}_c [M_\odot]$	1.06 ± 0.2
σ_{rms}	0.0166	$\mathcal{R}_h [R_\odot]$	4.48 ± 0.2	σ_{rms}	0.0409	$\mathcal{R}_h [R_\odot]$	4.48 ± 0.2
$i [^\circ]$	85.4 ± 0.2	$\mathcal{R}_c [R_\odot]$	16.6 ± 0.2	$i [^\circ]$	85.5 ± 0.3	$\mathcal{R}_c [R_\odot]$	16.6 ± 0.2
F_d	0.816 ± 0.03	$\log g_h$	3.82 ± 0.1	F_d	0.99 ± 0.03	$\log g_h$	3.82 ± 0.1
$T_d [K]$	2970 ± 200	$\log g_c$	2.02 ± 0.1	$T_d [K]$	3560 ± 300	$\log g_c$	2.02 ± 0.1
$d_e [a_{\text{orb}}]$	0.045 ± 0.005	M_{bol}^h	-2.24 ± 0.2	$d_e [a_{\text{orb}}]$	0.163 ± 0.006	M_{bol}^h	-2.31 ± 0.2
$d_c [a_{\text{orb}}]$	0.073 ± 0.005	M_{bol}^c	-0.13 ± 0.1	$d_c [a_{\text{orb}}]$	0.032 ± 0.007	M_{bol}^c	-0.13 ± 0.1
a_T	7.7 ± 0.3	$a_{\text{orb}} [R_\odot]$	64.6 ± 0.3	a_T	7.4 ± 0.4	$a_{\text{orb}} [R_\odot]$	64.6 ± 0.3
f_h	36.5 ± 0.5	$\mathcal{R}_d [R_\odot]$	27.4 ± 0.3	f_h	36.4 ± 0.5	$\mathcal{R}_d [R_\odot]$	33.2 ± 0.3
F_h	1.000	$d_e [R_\odot]$	2.9 ± 0.2	F_h	1.000	$d_e [R_\odot]$	10.5 ± 0.3
$T_h [K]$	14080 ± 500	$d_c [R_\odot]$	4.7 ± 0.2	$T_h [K]$	13990 ± 500	$d_c [R_\odot]$	2.0 ± 0.3
$A_{\text{hs}} = T_{\text{hs}}/T_d$	1.48 ± 0.05			$A_{\text{hs}} = T_{\text{hs}}/T_d$	1.13 ± 0.03		
$\theta_{\text{hs}} [^\circ]$	18.8 ± 2.5			$\theta_{\text{hs}} [^\circ]$	14.9 ± 2.6		
$\lambda_{\text{hs}} [^\circ]$	313.0 ± 6.0			$\lambda_{\text{hs}} [^\circ]$	314.6 ± 7.0		
$\theta_{\text{rad}} [^\circ]$	7.7 ± 7.0			$\theta_{\text{rad}} [^\circ]$	12.5 ± 7.0		
$A_{\text{bs}} = T_{\text{bs}}/T_d$	1.37 ± 0.04			$A_{\text{bs}} = T_{\text{bs}}/T_d$	1.08 ± 0.03		
$\theta_{\text{bs}} [^\circ]$	47.2 ± 8.0			$\theta_{\text{bs}} [^\circ]$	21.9 ± 3.0		
$\lambda_{\text{bs}} [^\circ]$	66.2 ± 9.0			$\lambda_{\text{bs}} [^\circ]$	125.4 ± 9.0		
Ω_h	17.848 ± 0.02			Ω_h	17.838 ± 0.03		
Ω_c	2.282 ± 0.02			Ω_c	2.282 ± 0.02		

FIXED PARAMETERS: $q = \mathcal{M}_c/\mathcal{M}_h = 0.22$ - mass ratio of the components, $T_c = 4400K$ - temperature of the less massive (cooler) donor, $F_c = 1.0$ - filling factor for the critical Roche lobe of the donor, $f_c = 1.00$ - non-synchronous rotation coefficients of the donor, $F_h = R_h/R_{zc}$ - filling factor for the critical non-synchronous lobe of the hotter, more massive gainer (ratio of the stellar polar radius to the critical Roche lobe radius along z-axis for a star in critical non-synchronous rotation regime), $\beta_h = 0.25$, $\beta_c = 0.08$ - gravity-darkening coefficients of the components, $A_h = 1.0$, $A_c = 0.5$ - albedo coefficients of the components. NOTE: n - number of observations, $\Sigma(O - C)^2$ - final sum of squares of residuals between observed (LCO) and synthetic (LCC) light-curves, σ_{rms} - root-mean-square of the residuals, i - orbit inclination (in arc degrees), $F_d = R_d/R_{yc}$ - disk dimension factor (the ratio of the disk radius to the critical Roche lobe radius along y-axis), T_d - disk-edge temperature, d_e , d_c - disk thicknesses (at the edge and at the center of the disk, respectively) in the units of the distance between the components, a_T - disk temperature distribution coefficient, f_h - non-synchronous rotation coefficient of the more massive gainer (in the critical non-synchronous rotation regime), T_h - temperature of the gainer, $A_{\text{hs,bs}} = T_{\text{hs,bs}}/T_d$ - hot spot temperature coefficients, $\theta_{\text{hs,bs}}$ and $\lambda_{\text{hs,bs}}$ - spot angular dimension and longitude (in arc degrees), θ_{rad} - angle between the line perpendicular to the local disk edge surface and the direction of the hot-spot maximum radiation, $\Omega_{h,c}$ - dimensionless surface potentials of the hotter gainer and cooler donor, $\mathcal{M}_{h,c} [M_\odot]$, $\mathcal{R}_{h,c} [R_\odot]$ - stellar masses and mean radii of stars in solar units, $\log g_{h,c}$ - logarithm (base 10) of the system components effective gravity, $M_{\text{bol}}^{h,c}$ - absolute stellar bolometric magnitudes, $a_{\text{orb}} [R_\odot]$, $\mathcal{R}_d [R_\odot]$, $d_e [R_\odot]$, $d_c [R_\odot]$ - orbital semi-major axis, disk radius and disk thicknesses at its edge and center, respectively, given in solar units.

Mennickent R. E., Schleicher D. R. G., San Martin-Perez R., 2018, PASP, 130, 94203

Mennickent R. E., et al., 2019, MNRAS, 487, 4169

Nataf D. M., et al., 2013, ApJ, 769, 88

Navarrete F. H., Schleicher D. R. G., Zamponi Fuentealba J., Völschow M., 2018, A&A, 615, A81

Packet, W. 1981, A&A, 102, 17

Paczynski B., 1977, ApJ, 216, 822

Pawlak, M., Graczyk, D., Soszyński, I., Pietrukowicz, P., Poleski, R., Udalski, A., Szymański, M. K., Kubiak, M., Pietrzyński, G., Wyrzykowski, Ł., Ulaczyk, K., Kozłowski, S., Skowron, J. 2013, Acta Astron, 63, 323

Percy, J. R., Matthews, J. M., & Wade, J. D. 1980, A&A, 82, 172

Poleski R., et al., 2010, AcA, 60, 179

Recio-Blanco A., et al., 2014, A&A, 567, A5

Richards M. T., 2004, AN, 325, 229

Scargle J. D., 1982, ApJ, 263, 835

Article number, page 8 of 8

Schleicher, D. R. G., & Mennickent, R. E. 2017, A&A, 602, A109

Soszyński, I., Pawlak, M., Pietrukowicz, P., Udalski, A., Szymański, M. K., Wyrzykowski, Ł., Ulaczyk, K., Poleski, R., Kozłowski, S., Skowron, D. M., Skowron, J., Mróz, P., Hamałowicz, A. 2016, Acta Astron, 66, 405

Steehls D., Horne K., Marsh T. R., Donati J. F., 1996, MNRAS, 281, 626

Sterken C., 2005, ASPC, 3, ASPC..335

Skulskij M. Y., 1982, SvAL, 8, 126

Skulskij M. Y., 2018, CoSka, 48, 300

Szymański M. K. 2005, AcA, 55, 43

Terrell D., Wilson R. E., 2005, Ap&SS, 296, 221

Udalski A., Szymański M. K. & Szymański G. 2015, AcA, 65, 1

Warner B., 1995a, Cambridge Astrophysics Series, 28

Zechmeister M., Kürster M., 2009, A&A, 496, 577